Optical spectroscopy of $SrWO_4:Nd^{3+}$ single crystals

2004 J. Phys.: Condens. Matter 16 6867

(http://iopscience.iop.org/0953-8984/16/39/019)

INSTITUTE OF PHYSICS PUBLISHING JOURNAL OF PHYSICS: CONDENSED MATTER

J. Phys.: Condens. Matter **16** (2004) 6867–6876 PII: S0953-8984(04)81041-5

Optical spectroscopy of $SrWO_4$:Nd^{3+} single crystals

Francesco Cornacchia[1], Alessandra Toncelli[1], Mauro Tonelli[1], Enrico Cavalli[2], Enrico Bovero[2] and Nicola Magnani[3]

[1] NEST-INFM and Dipartimento di Fisica, Università di Pisa, Via Buonarroti 2, 56127 Pisa, Italy
[2] INFM and Dipartimento di Chimica Generale ed Inorganica, Chimica Analitica e Chimica Fisica, Università di Parma, Viale delle Scienze 17/a, 43100 Parma, Italy
[3] INFM and Dipartimento di Fisica, Università di Parma, Viale delle Scienze 15, 43100 Parma, Italy

E-mail: francesco.cornacchia@df.unipi.it and enrico.cavalli@unipr.it

Received 20 May 2004
Published 17 September 2004
Online at stacks.iop.org/JPhysCM/16/6867
doi:10.1088/0953-8984/16/39/019

Abstract

The optical properties of $SrWO_4$ crystals doped with Nd^{3+} have been investigated at temperatures ranging from 10 to 300 K. The scheme of the energy levels up to 20 000 cm^{-1} has been deduced from low temperature measurements and reproduced by theoretical calculations based on a parametric Hamiltonian including Coulombic, spin–orbit and crystal field terms. The spontaneous transition probabilities, the branching ratios and the radiative lifetime have been calculated in the framework of the Judd–Ofelt theory and compared with the experimental results for the $^4F_{3/2}$ emitting level. The optical bands are broadened because of crystal field inhomogeneities caused by charge compensation processes accompanying the substitution of Nd^{3+} for Sr^{2+}. This fact and the high emission cross section values obtained for the emission from the $^4F_{3/2}$ multiplet indicate Nd:$SrWO_4$ as a possible active medium for tunable laser operation.

1. Introduction

Tungstates and molybdates with the scheelite structure constitute a family of crystals suitable for stimulated Raman scattering (SRS) operation and have been thoroughly studied in order to develop laser devices emitting in new spectral regions [1]. Doping with luminescent ions, such as Nd^{3+}, yields special laser materials where the Raman properties of the host lattice are combined with the emission properties induced by the active ions. Neodymium-doped scheelite-type crystals (including $SrWO_4$) were briefly studied in the 1960s [2]; the crystal growth conditions and the stimulated emission properties of Nd^{3+}-doped $SrWO_4$ have been recently investigated in [3], where it was demonstrated that this is an attractive multifunctional

laser medium. However, no information is given about the spectroscopic properties of this material, which are important for assessing its best operating conditions and also for comparison with other laser crystals based on the Nd^{3+} ion. We have measured the 10 and 298 K absorption and emission spectra and the decay curves as a function of the temperature of Nd:$SrWO_4$ at two different doping levels. All the observed spectral features show a marked inhomogeneous broadening. From the low temperature data we have obtained the order and the structure of the energy levels. The room temperature absorption spectra have been analysed using the Judd–Ofelt approach, and the intensity parameters, the branching ratios and the radiative lifetime of the $^4F_{3/2}$ emitting level have been evaluated. These values have been compared with the results obtained from the measurements of the fluorescence decay after pulsed excitation, in order to estimate the importance of the non-radiative processes. We have also calculated, from our experimental data, the polarized stimulated emission cross sections, in order to estimate the potentialities of the title compound as regards technological applications.

2. Experimental details

Nd:$SrWO_4$ crystals with 1.2% and 12% Nd/Sr nominal molar ratios (corresponding to 6.2×10^{19} and 6.2×10^{20} ions cm^{-3} respectively) were grown by the 'flux growth' technique [4]. The starting mixtures, constituted of suitable amounts of reagent grade $SrCO_3$, WO_3, Na_2WO_4, $Na_2B_4O_7$ and Nd_2O_3, were put in platinum crucibles and slowly heated to 1250 °C in a horizontal furnace under an air atmosphere. After a soaking time of 12 h the temperature was lowered to 800 °C with a cooling rate of 2 °C h^{-1}. Then the furnace was turned off. Well formed, blue crystals up to $4 \times 3 \times 2$ mm^3 were separated by leaching with a hot diluted NaOH solution. ICP experiments carried out in order to determine the actual Nd^{3+} doping levels in the crystals did not produce reliable results because of problems in the solubilization of the samples. Therefore for all the measurements and analysis the Nd concentration has been assumed equal to the nominal one; the validity of this assumption will be discussed in section 5. The crystal structure was checked by x-ray diffraction (XRD) techniques.

The samples for the spectroscopic measurements were oriented by the x-ray Laue technique, cut and optically polished with alumina powder in order to investigate polarization-dependent optical properties. Typical dimensions for polished crystals were $2 \times 2 \times 1$ mm^3. The absorption spectra were recorded with a spectroscopic system equipped with a 300 W halogen lamp fitted with a 0.25 m Spex monochromator as the source, using a Glan–Thomson prism to polarize the incident radiation. The output radiation was analysed by means of a 1.26 m Spex monochromator and detected with a RCA C31034 photomultiplier or an NEP PbS detector. The resolution of the absorption spectra was better than 0.2 nm in the visible and 2 nm in the NIR region.

The samples were mounted onto the cold finger of a closed cycle He cryostat and all the measurements were carried out at temperatures ranging from 10 to 300 K. The room temperature fluorescence spectra were measured by exciting the sample with a home-made cw tunable Ti:Al_2O_3 laser (pumped by an Ar^+ laser), tuned at 804 nm. The emission was collected perpendicularly to the pump laser direction to avoid spurious pump scattering, chopped and focused on the input slit of a monochromator with 25 cm focal length equipped with a grating with 600 g mm^{-1} blazed at 1 μm, with a resolution of 1.8 nm. In order to perform polarization-dependent measurements we placed a Glan–Thomson polarizer in front of the input slit of the monochromator and suitable filters to completely suppress any laser scattering from the samples. The signal was detected by a liquid nitrogen cooled InSb detector, fed into pre-amplifiers, processed by a lock-in amplifier and stored on a PC. All the spectra were corrected for the optical response of the apparatus.

For room temperature fluorescence lifetime measurements of the $^4F_{3/2}$ manifold the samples were excited by a pulsed tunable Ti:Al_2O_3 laser with 10 Hz repetition rate, 30 ns pulse width. In order to observe a uniformly pumped volume and to reduce radiation trapping, we collected the fluorescence from a short portion ($\approx$1 mm thick) of the sample; furthermore, the power incident on the fibres was reduced as much as possible by means of an attenuator to minimize non-linear effects. The signal was detected by the same experimental apparatus as described above, but the detector was a S1 cathode photomultiplier and the signal was sent, by a fast amplifier, to a digital oscilloscope connected to a computer. The response time of the system was about 1 μs.

3. Structural data and absorption spectroscopy

$SrWO_4$ has the tetragonal scheelite ($CaWO_4$) structure [4], with space group $I4_1/a$ and cell parameters $a = 5.417$ Å and $c = 11.951$ Å. The Nd^{3+} doping ions replace the Sr^{2+} ones in sites with eightfold oxygen coordination (distorted dodecahedron, actual point group S_4). The subsequent excess of charge is compensated by the accommodation of Na^+ ions present in the growth mixture and/or by the formation of cation vacancies. These charge compensation mechanisms produce slight differences in the spatial distributions around the active ions and then in the local fields acting on them, and this will result in the inhomogeneous broadening of the absorption and emission features observed in the optical spectra even at low temperature.

The 10 and 300 K polarized absorption spectra of Nd:$SrWO_4$ (12%) measured in the 360–900 nm range are shown in figure 1. The 10 K spectra are made up of manifolds whose structure and polarization behaviour arise from the crystal field (CF) lifting of the degeneracies of the states belonging to the $4f^3$ electronic configuration of the Nd^{3+} ion. In fact, the coordination geometry around the optically active centre induces the splitting of $^{2S+1}L_J$ states of the free ion into Stark levels transforming according to the $\Gamma_5 + \Gamma_6$ (hereafter denoted as $\Gamma_{5,6}$) or $\Gamma_7 + \Gamma_8$ ($\Gamma_{7,8}$) irreducible representations of the S_4 symmetry point group [5]. The selection rules for the electric dipole allowed transitions are then

$$\begin{array}{ll} \sigma & \begin{cases} \Gamma_{5,6} \rightarrow \Gamma_{6,5} \\ \Gamma_{7,8} \rightarrow \Gamma_{8,7} \end{cases} \\ \sigma, \pi & \begin{cases} \Gamma_{5,6} \rightarrow \Gamma_{7,8} \\ \Gamma_{7,8} \rightarrow \Gamma_{5,6} \end{cases} \end{array} \tag{1}$$

where σ and π indicate the orientation of the electric vector E of the radiation with respect to the crystallographic c axis ($\sigma \rightarrow E \perp c$, $\pi \rightarrow E \parallel c$). On this basis we have analysed the structure of the multiplets and assigned most of the observed transitions according to the energy level diagram given in many previous investigations [6, 7].

Using the energy values deduced from the NIR absorption spectra for the $^4I_{15/2}$ state and from the fluorescence data (shown in the next section) for the lowest levels, we have been able to complete the scheme of the energy levels of the optically active ion from 0 up to 20 000 cm^{-1}. This is reported in table 1.

The observed energy values were then reproduced using a Hamiltonian of the form

$$H = H_{\mathrm{FI}} + H_{\mathrm{CF}} \tag{2}$$

where the free-ion part H_{FI} is written as [8, 9]

$$H_{\mathrm{FI}} = E_{\mathrm{av}} + \sum_k F^k f_k + \zeta H_{so} + \alpha L(L+1) + \beta G(G_2) + \gamma G(R_7) + \sum_i T^i t_i + \sum_j M^j m_j + \sum_k P^k p_k \tag{3}$$

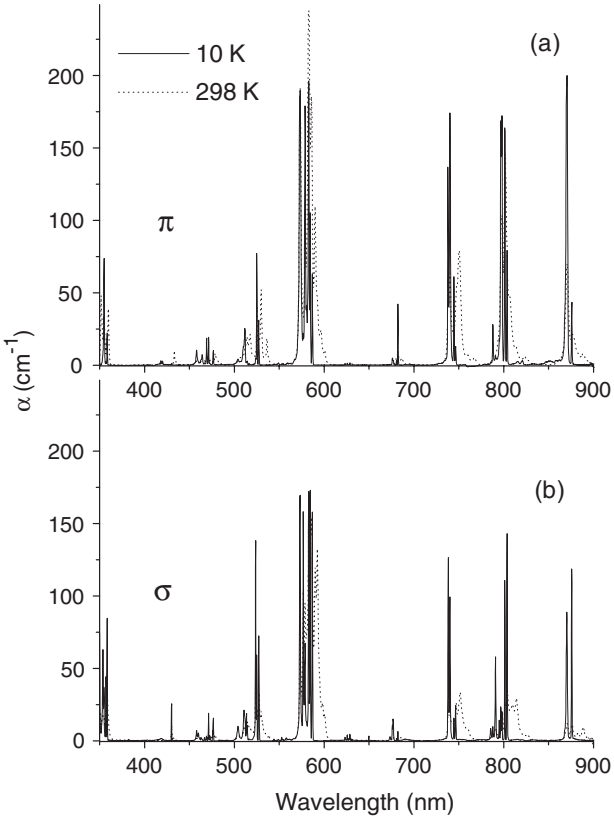

Figure 1. The 10 and 300 K polarized absorption spectra of Nd:$SrWO_4$ (12%) measured in the 360–900 nm range.

where $k = 2, 4, 6$, $i = 2, 3, 4, 6, 7, 8$, $j = 0, 2, 4$, and the crystal field Hamiltonian H_{CF} can be expressed in terms of tensor operators [10]:

$$H_{\mathrm{CF}} = \sum_{q,k} B_k^q C_q^k. \tag{4}$$

In S_4 symmetry it can be expanded to the form

$$H_{\mathrm{CF}} = B_2^0 C_0^2 + B_4^0 C_0^4 + B_4^4 [C_4^4 + C_{-4}^4] + B_6^0 C_0^6 + B_6^4 [C_4^6 + C_{-4}^6]. \tag{5}$$

This model Hamiltonian accounts for two-body electrostatic repulsion (F^k), two- and three-body configuration interactions (α, β, γ and T^i, respectively), spin–orbit coupling (ζ), spin–other-orbit interactions (M^j), electrostatically correlated spin–orbit interactions (P^k) and the crystal field potential. A detailed description of the various free-ion operators and parameters is available in the literature [9]; the tensor operators are defined in [10]. The procedure used for the calculations is essentially that described in [8]. Most of the 19 free-ion parameters (all except F^2, F^4, F^6 and ζ) were kept fixed during the fitting procedure; in contrast, all the crystal field parameters allowed by the S_4 point group symmetry (B_2^0, B_4^0, B_6^0, B_4^4 and B_6^4) were freely varied. Following the usual convention we fixed the rotational degree of freedom by assuming B_4^4 to be real and positive and letting B_6^4 have complex values. Two different sets of crystal field parameters, obtained from the literature and referred to Nd^{3+} embedded in the isostructural compounds $CaWO_4$ [11] and $NaLa(MoO_4)_2$ [12], were used as starting points; in both cases the fitting quickly converged to almost the same B_q^k values. The best fit of the experimental data was obtained using the parameters reported in table 2; as

Table 1. Energy levels of Nd^{3+} in $SrWO_4$. Experimental and theoretical values (calculated using equation (3)) are reported.

$^{2S+1}L_J$	Γ	E_{calc} (cm^{-1})	E_{exp} (cm^{-1})	ΔE (cm^{-1})	$^{2S+1}L_J$	Γ	E_{calc} (cm^{-1})	E_{exp} (cm^{-1})	ΔE (cm^{-1})
	7, 8	−3	0	3		7, 8	13 398	13 398	0
	7, 8	100	91	−9	$^4F_{7/2}$	5, 6	13 433	13 430	−3
$^4I_{9/2}$	5, 6	170	155	−15	+	7, 8	13 509	13 512	3
	5, 6	221	218	−3	$^4S_{3/2}$	5, 6	13 518	—	—
	7, 8	405	396	−9		5, 6	13 529	13 546	17
						7, 8	13 559	13 554	−5
	7, 8	1 956	1 956	6					
	5, 6	1 992	1 999	7		5, 6	14 667	14 658	−9
$^4I_{11/2}$	7, 8	2 001	2 008	7		7, 8	14 690	14 690	0
	5, 6	2 037	2 045	8	$^4F_{9/2}$	5, 6	14 765	14 775	10
	5, 6	2 139	2 150	11		7, 8	14 769	14 793	24
	7, 8	2 170	2 179	9		7, 8	14 840	14 852	12
	5, 6	3 911	3 894	−17		5, 6	15 916	15 910	−6
	7, 8	3 945	3 932	−13		7, 8	15 918	15 929	11
	5, 6	3 950	3 962	12	$^2H_{11/2}$	7, 8	15 938	15 931	−7
$^4I_{13/2}$	7, 8	3 996	—	—		5, 6	15 946	15 948	2
	5, 6	4 115	4 121	6		7, 8	15 961	—	—
	5, 6	4 141	4 132	−9		5, 6	15 990	15 979	−11
	7, 8	4 150	4 146	−4					
						5, 6	17 111	17 111	0
	5, 6	5 853	5 855	2		7, 8	17 164	17 158	−6
	5, 6	5 907	5 907	0	$^4G_{5/2}$	5, 6	17 213	17 229	16
	7, 8	5 941	5 942	1	+	7, 8	17 280	17 277	−3
$^4I_{15/2}$	7, 8	6 016	6 013	−3	$^2G_{7/2}$	5, 6	17 286	17 289	3
	7, 8	6 218	—	—		7, 8	17 349	17 337	−12
	5, 6	6 246	6 242	−4		5, 6	17 470	17 446	−24
	7, 8	6 267	—	—					
	5, 6	6 308	6 309	1		7, 8	18 979	18 968	−11
					$^4G_{7/2}$	5, 6	19 008	19 048	40
$^4F_{3/2}$	7, 8	11 428	11 421	−7		5, 6	19 091	19 091	0
	5, 6	11 499	11 492	−7		7, 8	19 134	19 148	14
	7, 8	12 442	12 444	2		7, 8	19 391	19 372	−19
	5, 6	12 489	12 475	−14		5, 6	19 439	19 433	−6
	7, 8	12 523	12 531	8		7, 8	19 490	19 470	−20
$^4F_{5/2}$	5, 6	12 553	12 550	−3	$^4G_{9/2}$	5, 6	19 505	—	—
+	5, 6	12 564	12 578	14	+	5, 6	19 533	19 539	6
$^2H_{9/2}$	5, 6	12 643	12 645	2	$^2K_{13/2}$	7, 8	19 557	19 555	−2
	7, 8	12 663	12 691	28		7, 8	19 574	19 577	3
	7, 8	12 731	12 732	1		5, 6	19 580	19 585	5
						5, 6	19 606	19 600	−6
						7, 8	19 618	19 610	−8
						7, 8	19 826	19 825	−1
						5, 6	19 829	19 841	12

one might reasonably expect, they are quite a lot more similar to those of $CaWO_4$ than to those of $NaLa(MoO_4)_2$. The calculated energy levels are listed in table 1, where they are compared

Table 2. Parameters used in equation (3) to obtain the theoretical energy levels of table 1.

Parameter	cm^{-1}	Parameter	cm^{-1}
E_{av}	24 233	ζ	883
F_2	72 204	M_0	2.11
F_4	52 596	M_2	1.18
F_6	35 280	M_4	0.65
α	21.3	P_2	192
β	−593	P_4	96
γ	1445	P_6	19
T_2	298	B_2^0	571
T_3	35	B_4^0	−674
T_4	59	B_6^0	−119
T_6	−285	B_4^4	869
T_7	332	B_6^4	808 + 5i
T_8	305	rms	11.3

with the experimental values. The overall rms value of 11.3 cm^{-1} is satisfactory, being of the same order as the observed linewidths.

It is interesting to note that the transition $^4I_{9/2} \rightarrow {}^2P_{1/2}$ at 10 K consists of a single line, and therefore its linewidth reflects the inhomogeneous broadening induced by the presence of disorder [13]. In the case of Nd:$SrWO_4$, the full width at half-maximum (FWHM) of this absorption band is about 25 cm^{-1}, a value which is only 4–5 times less than that observed for oxide glasses [14]. This expected behaviour is common among crystals where the local inhomogeneities of the crystal field around the optically active ion induce broadening of the absorption and emission features, as pointed out before. On passing to room temperature, a number of 'hot bands' appear, connected to the transitions from the thermally populated upper components of the $^4I_{9/2}$ ground state and, moreover, the components of the multiplets broaden, giving rise to broad bands. The absorption system in the 780–840 nm range, for example, is important for laser diode pumping. As can be seen in figure 2, in this region the π spectrum is more intense than the σ one and its FWHM (6.7 nm, corresponding to 114 cm^{-1}) is similar to the largest ones reported for laser crystals based on the Nd^{3+} ion [16].

4. Fluorescence spectroscopy and decay kinetics

The 10 and 300 K unpolarized emission spectra of the 1.2% doped sample in the 850–1100 nm region are shown in figure 3. The two band systems centred at about 880 and 1060 nm are assigned to the transitions from the $^4F_{3/2}$ level to the $^4I_{9/2}$ and $^4I_{11/2}$ manifolds, respectively, and correspond to the most important laser channels.

The 10 K $^4F_{3/2} \rightarrow {}^4I_{9/2}$ transition is made up of five components, as predicted from the complete Stark splitting of the $^4I_{9/2}$ ground level. The overall splitting of this level is of about 400 cm^{-1}, in agreement with that of other oxide crystals [6]. The most intense peak of this multiplet is centred at 887.6 nm with FWMH of 16 cm^{-1} and the lines at wavelengths longer than 890 nm are broader and less intense. On passing to 300 K the features of the manifolds broaden and collapse into a single broad band, even owing to the appearance of hot components.

The $^4F_{3/2} \rightarrow {}^4I_{11/2}$ transition shows the expected six components, the most intense one being at 1062.4 nm with FWMH of 18 cm^{-1}. As in the previous case, at $T = 300$ K this

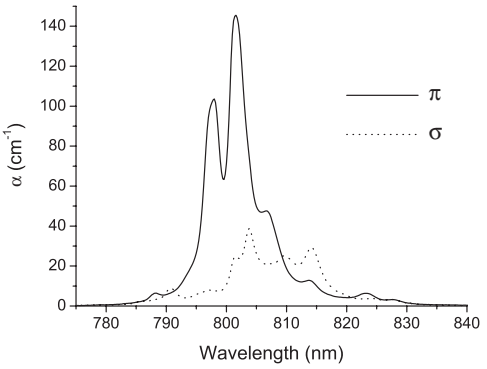

Figure 2. 300 K absorption spectra of the $^4F_{5/2} + {}^2H_{9/2}$ manifolds of Nd^{3+} in $SrWO_4$ (12% doping density).

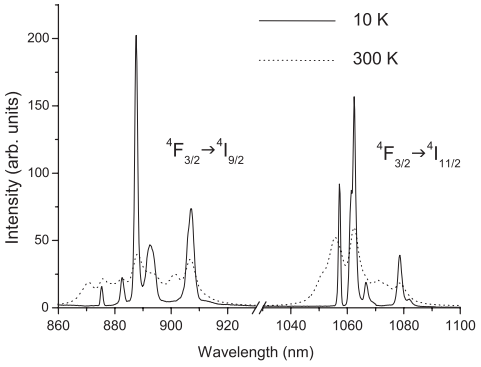

Figure 3. The 10 and 300 K unpolarized emission spectra of the 1.2% doped sample in the 850–1100 nm region.

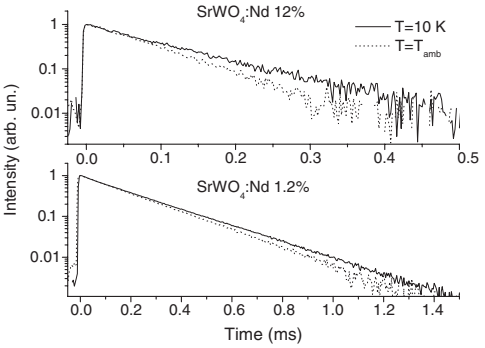

Figure 4. Decay curves of the $^4F_{3/2}$ Nd^{3+} manifold in $SrWO_4$.

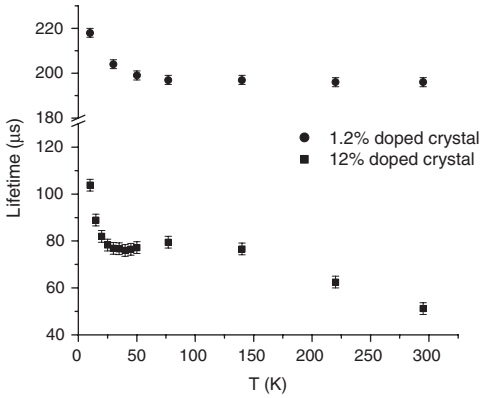

Figure 5. The decay time of the $^4F_{3/2}$ Nd^{3+} manifold in $SrWO_4$. In the figure, ● is used for the 1.2% doped sample and ■ for the 12% doped crystal.

emission system broadens up into a single broad band extending from 1040 to 1090 nm. This behaviour makes Nd:$SrWO_4$ an interesting candidate for tunable solid state laser operation.

A similar behaviour has been observed for the weaker $^4F_{3/2} \rightarrow {}^4I_{13/2}$ transition, located at about 1.35 μm and not shown here for brevity.

We measured the decay curves of the fluorescence from $^4F_{3/2}$ at 880 nm of both 1.2% and 12% doped crystals as a function of the temperature. Pulsed excitation gives rise to exponential decay profiles independently of the temperature, as can be observed in figure 4 where the 10 and 300 K curves of both crystals are reported. The measured lifetime of the slightly doped crystal is 218 μs at 10 K (in agreement with the value found in [2]), decreasing to 195 μs at 300 K, whereas that of the heavily doped sample ranges from 105 μs at 10 K to 45 μs at 300 K. The temperature dependences of the lifetimes are shown in figure 5. In the case of the diluted crystal the decrease with temperature can be tentatively attributed to the thermal population of the two components of the $^4F_{3/2}$ emitting level. Therefore in the temperature range considered the non-radiative processes are ineffective, in agreement with the fact that the energy gap between the emitting level and the next lower $^4I_{15/2}$ state, about 5100 cm^{-1}, is more than five times the maximum phonon energy of the host (920 cm^{-1}) [1, 15]. The lifetimes of the

Table 3. Experimental and calculated oscillator strengths (P) of Nd^{3+} in $SrWO_4$. The Judd–Ofelt parameters Ω_l, the rms and the percentage error are also reported. (Note: $\Omega_2 = 12.49 \times 10^{-20}$ cm^2, $\Omega_4 = 5.72 \times 10^{-20}$ cm^2, $\Omega_6 = 4.39 \times 10^{-20}$ cm^2. rms $= 1.59 \times 10^6$, error $= 14\%$.)

Excited state	Barycentre (cm^{-1})	P_{exp} (10^6)	P_{calc} (10^6)
$^4F_{3/2}$	11 395	2.70	3.45
$^4F_{5/2} + {}^2H_{9/2}$	12 411	9.68	9.13
$^4F_{7/2} + {}^4S_{3/2}$	13 368	7.57	8.24
$^4F_{9/2}$	14 643	3.99	0.70
$^4G_{5/2} + {}^2G_{7/2}$	17 115	52.8	52.9
$^4G_{7/2} + {}^4G_{9/2} + {}^2K_{13/2}$	19 131	10.3	9.82
$^2G_{9/2} + {}^2D_{3/2} + {}^4G_{11/2} + {}^2K_{15/2}$	21 169	2.08	1.75
$^2P_{1/2}$	23 146	0.54	0.95

concentrated crystals are evidently affected by concentration quenching probably connected to energy transfer processes and to the presence of 'killer' centres, whose effectiveness increases with the temperature thanks to phonon assistance. This information is useful for optimizing the doping level in crystals for technological applications.

5. Judd–Ofelt analysis and laser parameters

A Judd–Ofelt [17, 18] analysis was carried out for the room temperature absorption of the 12% doped sample shown in figure 1. Eight bands were considered to calculate the intensity parameters Ω_l ($l = 2, 4, 6$); we did not take into account the $^4I_{9/2} \rightarrow {}^2H_{11/2}$ transition because its intensity is negligible. The oscillator strengths of the transitions were reliably determined by considering the contributions of the two different polarizations with a 2:1 ratio for $\sigma:\pi$, and the experimental data were fitted on the basis of the JO parametrization scheme after subtraction of the magnetic dipole contribution for the $^4I_{9/2} \rightarrow {}^2H_{9/2}$, $^4I_{9/2} \rightarrow {}^4F_{9/2}$, $^4I_{9/2} \rightarrow {}^2G_{7/2}$ and the $^4I_{9/2} \rightarrow {}^4I_{11/2}$ transitions. These contributions are small and not reported here. The reduced matrix elements were taken from [7], and the value of the refractive index was assumed to be $n = 1.87$, in agreement with the value reported for the similar $CaWO_4$ crystal [19]. The calculated oscillator strengths, the intensity parameters and the root mean square deviation (rms) are reported in table 3. The high value of the parameter Ω_2 accounts for the high oscillator strength of the hypersensitive $^4I_{9/2} \rightarrow {}^4G_{5/2} + {}^2G_{7/2}$ absorption transition and for the temperature behaviour of some its components, which in the π spectrum are more intense at 300 K than at 10 K as a consequence of their strong sensitivity to the variations of their surroundings [20]. This has no practical effect on the emission properties of the title compound from the $^4F_{3/2}$ state, as they mainly depend on the parameters Ω_4 and Ω_6 [6, 7]. These are similar to the values found for the most common laser materials based on the Nd^{3+} ion, such as YAG, YVO_4 and others [7]. The calculated spontaneous emission probabilities and the radiative branching ratios for the transitions from the $^4F_{3/2}$ state to the components of the ^4I_J ($J = 15/2, 13/2, 11/2, 9/2$) manifold are reported in table 4, together with the radiative lifetime of the emitting level. They were estimated using the calculated intensity parameters and the reduced matrix elements published in [7] and correcting for the refractive index; furthermore, in table 4 we give the experimental value of the branching ratios obtained from the fluorescence spectra. The resulting radiative lifetime, 184 μs, is in reasonable agreement with the measured values reported in section 4 for the 1.2% doped crystal. This confirms that the non-radiative processes are ineffective at low Nd^{3+} concentrations and that the actual doping density can be assumed equal to the nominal one, especially considering the intrinsic error

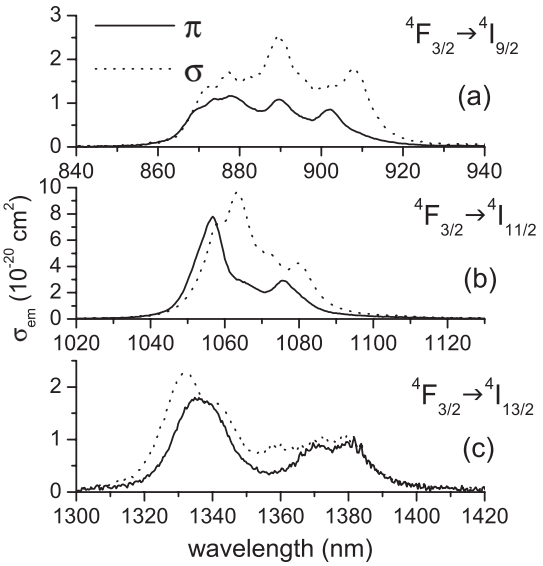

Figure 6. Polarized emission cross sections of the transitions originating from $^4F_{3/2}$.

Table 4. Calculated spontaneous emission probabilities A, calculated and experimental branching ratios (β_{calc}, β_{exp}) and calculated radiative lifetimes τ_{calc} of the $^4F_{3/2}$ Nd^{3+} multiplet in $SrWO_4$.

Initial state	Final state	A (s^{-1})	β_{calc}	β_{exp}	τ_{calc} (μs)
$^4F_{3/2}$	$^4I_{15/2}$	22.6	0.004	0	
	$^4I_{13/2}$	438.1	0.08	0.09	184
	$^4I_{11/2}$	2380	0.440	0.53	
	$^4I_{9/2}$	2580	0.475	0.38	

of the Judd–Ofelt analysis, of the order of 20%. The good agreement between the calculated and observed data confirms the reliability of the calculations carried out using the nominal concentration.

The stimulated emission cross section (σ_{em}) was evaluated using the $\beta-\tau$ method [21] for the emission transitions from $^4F_{3/2}$ to the ^4I_J ($J = 13/2, 11/2, 9/2$) manifolds at room temperature in order to ascertain the potentialities of the present material for research and for industrial applications. In figure 6 the σ_{em} at room temperature for the three transitions are shown for the two crystal orientations $E \parallel c$ (π) and $E \perp c$ (σ). The $^4F_{3/2} \rightarrow {}^4I_{9/2}$ transition in the 900 nm wavelength region, shown in figure 6(a), is characterized by a broad emission. The FWHM of this band is about 530 cm^{-1} (42 nm). The peak values of the emission cross section are 2.6×10^{-20} cm^2 for σ orientation and 1.1×10^{-20} cm^2 for π orientation at 889 nm. We think that the laser emission is more likely in the long wavelength region of the emission because of strong ground state absorption in this region. The most important Nd^{3+} transition ($^4F_{3/2} \rightarrow {}^4I_{11/2}$) is shown in figure 6(b). It consists of a single broad emission band whose FWHM is about 250 cm^{-1} (28 nm). The emission cross sections are 9.7×10^{-20} cm^2 at 1063 nm for the σ polarization and 7.8×10^{-20} cm^2 at 1056 nm for the π one. These values indicate that Nd:$SrWO_4$ is a quite promising candidate for tunable solid state laser operation in the 1.06 mm region. Figure 6(c) shows the 1350 nm wavelength region corresponding to the $^4F_{3/2} \rightarrow {}^4I_{13/2}$ transition. It is a broad emission band typical of disordered crystals and its intensity maximum is at 1332 nm, with a FWHM of 23 nm. The σ_{em} at this wavelength is 1.6 and 2.2×10^{-20} cm^2 for the π and σ polarizations, respectively. These values are

only two times lower than the ones obtained for Nd:YAG crystals [22] but the FWHM for the $^4F_{3/2} \rightarrow {}^4I_{11/2}$ transition is larger than or comparable with the values for other disordered crystals such as KLM [16] (≈22 nm) CNGG [23] (17 nm) and CaSGG [24] (≈22 nm).

6. Conclusion

The optical spectra of the Nd:$SrWO_4$ laser crystal have been investigated at 10 and 300 K. The low temperature data allowed us to obtain the scheme for the lower lying levels of the Nd^{3+} ion, whose energy values have been reliably reproduced by a standard theoretical calculation. The room temperature absorption spectra have been analysed in the framework of the Judd–Ofelt theory: the calculated intensity parameters are consistent with those reported for other laser materials based on the Nd^{3+} ion [7]. The comparison between the calculated and the measured lifetimes indicates that the non-radiative processes are nearly inefficient in the case of the diluted crystals, whereas they significantly affect the emission efficiency in the case of the 12% doped sample. Finally, the large absorption coefficient in the 800 nm region and the broadband character of the absorption and emission features make the title compound particularly promising from the perspective of developing a completely solid state tunable laser in the 1.06 and 1.35 μm regions.

Acknowledgment

The authors wish to thank Mrs Ilaria Grassini for the optical preparation of the samples.

References

[1] Basiev T T, Sobol A A, Voronko Y K and Zverev P G 2000 *Opt. Mater.* **15** 205
[2] Morozov A M, Tolstoi M N and Feofilov P P 1967 *Opt. Spectrosc.* **22** 139
[3] Ivleva L I, Basiev T T, Voronin I S, Zverev P G, Osiko V V and Polozkov N M 2003 *Opt. Mater.* **23** 439
[4] Gürmen E, Daniels E and King J S 1971 *J. Chem. Phys.* **55** 1093
[5] Koster G F, Dimmock J O, Wheeler R G and Statz H 1963 *Properties of the Thirty-Two Point Groups* (Cambridge, MA: MIT Press)
[6] Kaminskii A A 1981 *Laser Crystals* (Berlin: Springer)
[7] Kaminskii A A 1996 *Crystalline Lasers: Physical Processes and Operating Schemes* (New York: CRC Press)
[8] Carnall W T, Goodman G L, Rajnak K and Rana R S 1989 *J. Chem. Phys.* **90** 3443
[9] Crosswhite H M and Crosswhite H 1984 *J. Opt. Soc. Am.* B **1** 246 and references therein
[10] Wybourne B G 1965 *Spectroscopic Properties of Rare Earths* (New York: Interscience)
[11] Karayianis N and Farrar R T 1970 *J. Chem. Phys.* **53** 3436
[12] Stevens S B, Morrison C A, Allik T H, Rheingold A L and Haggerty B S 1991 *Phys. Rev.* B **43** 7386
[13] Brecher C, Riseberg L A and Weber M J 1978 *Phys. Rev.* B **18** 5799
[14] Wacthler M, Speghini A, Gatterer K, Fritzer H P, Ajò D and Bettinelli M 1998 *J. Am. Ceram. Soc.* **81** 2045
[15] Christofilos D, Papagelis K, Ves S, Kovouklis G A and Raptis C 2002 *J. Phys.: Condens. Matter* **14** 12641
[16] Cavalli E, Zannoni E, Mucchino C, Carozzo V, Toncelli A, Tonelli M and Bettinelli M 1999 *J. Opt. Soc. Am.* B **16** 1958
[17] Judd B R 1962 *Phys. Rev.* **127** 750
[18] Ofelt G S 1962 *J. Chem. Phys.* **37** 511
[19] Voronina I S, Ivleva L I, Basiev T T, Zverev P G and Polozkov N M 2003 *J. Optoelectron. Adv. Mater.* **5** 887
[20] Peacock R D 1975 *The Intensities of Lanthanide $f \leftrightarrow f$ Transitions, in Struct. Bonding* p 83
[21] Aull B F and Jenssen H P 1982 *IEEE J. Quantum Electron.* **18** 925
[22] Kück S, Fornasiero L, Mix E and Huber G 1998 *OSA Trends in Optics and Photonics* (*Advanced Solid State Lasers* vol 19) ed W R Bosemberg and M M Fejer (Washington, DC: Optical Society of America) p 425
[23] Agnesi A, Dell'Acqua S, Guandalini A, Reali G, Cornacchia F, Toncelli A, Tonelli M, Shimamura K and Fukuda T 2001 *IEEE J. Quantum Electron.* **37** 304
[24] Cavalli E, Zannoni E, Belletti A, Carozzo V, Toncelli A, Tonelli M and Bettinelli M 1999 *Appl. Phys.* B **68** 677